Journal of The Electrochemical Society, 2023 **170** 090504
1945-7111/2023/170(9)/090504/10/$40.00 © 2023 The Electrochemical Society ("ECS"). Published on behalf of ECS by IOP Publishing Limited

Large Li-Ion Insertion Capacity of Thin-Wall Anatase TiO_2 Nanotubes at 25 °C–55 °C

Nemanja Latas[1] and **Nikola Cvjetićanin**[2,*,z]

[1] *University of Belgrade - Department of Atomic Physics, INS Vinča—National Institute of the Republic of Serbia, Mike Alasa 12-14, 11001 Belgrade, Serbia*
[2] *University of Belgrade—Faculty of Physical Chemistry, Studentski trg 12-16, 11158 Belgrade, Serbia*

Anatase TiO_2 was prepared in the form of nanotube arrays by anodic oxidation of Ti foil followed by annealing at 400 °C. Electrochemical experiments, which included cyclic voltammetry (CV), galvanostatic (GS) cycling and electrochemical impedance spectroscopy (EIS) were conducted in 1 M solution of $LiClO_4$ in propylene carbonate (PC) at temperatures 25 °C–55 °C. CV experiments, at scan rates 5–50 $mV{\cdot}s^{-1}$, demonstrated with increasing temperature a large increase in the intensity of the redox peaks along with a decrease in the peak-to-peak separation. GS cycling showed large increase of capacity of thin-wall TiO_2 nanotubes with increasing temperature, which attains 357 $mAh{\cdot}g^{-1}$ at 55 °C during lithiation at current rate 5.3 C, with capacity retention of 98.5% and Coulombic efficiency of 97.5%. Surface storage and development of secondary voltage plateau strongly contribute to such a large capacity value. EIS showed a multiple decrease in solid electrolyte interphase (SEI) layer resistance and charge transfer resistance with temperature rising up to 55 °C.
 [DOI: 10.1149/1945-7111/acf245]

Manuscript submitted June 17, 2023; revised manuscript received August 7, 2023. Published September 4, 2023.

Supplementary material for this article is available online

A higher demand for efficient storage devices has set a goal of improving the efficiency of lithium-ion batteries (LIBs), which are currently one of the most promising energy storage devices.[1–3] LIBs are nowadays known for powering numerous portable electronic appliances, while the hybrid electric vehicles (HEVs) and electric vehicles (EVs) industry is developing rapidly worldwide. Most recently these batteries have even been considered for applications in aerospace industry.[4] The diverse range of applications is the result of the lithium-based chemistry, light weight and long cycle-life.[5,6] Most of the commercial LIBs today are composed of lithium source cathodes based on transition metal oxides and phosphates paired with a graphite anode in the presence of an aprotic solvent.[7] However, it seems that the LIBs with graphite anode cannot meet the future requirements of high performance and fast rechargeability due to the nature of solid electrolyte interphase (SEI) layer formed. In this context, there is an increased interest in developing novel anode materials, with enhanced kinetics. Several transition metal-oxide based insertion hosts, such as $Li_4Mo_5O_{17}$, V_3BO_6, $Li_4Ti_5O_{12}$, Nb_2O_5, $LiCrTiO_4$, TiO_2[8–17] and most recently $Mo_{1.5}W_{1.5}Nb_{14}O_{44}$[18] have been introduced as possible alternatives to the graphite anodes. A very important issue nowadays is the thermal management of LIBs, especially those for EVs.[19,20] At low temperatures (e.g. <15 °C) the slower diffusion of Li-ions in both electrolyte and electrodes and increase of charge transfer resistance affects capacity and power of these batteries. At high temperatures (e.g. >40 °C) the heat generated by LIB itself can cause overheating, which shortens the life of the battery due to PVDF binder migration and SEI layer increase. As a much more drastic result, combustion, explosion and release of toxic gases can occur. The management at low/high temperature issues is achieved through electrical, liquid and PCM (phase change material) heating/cooling of batteries. Regardless of the successful development of thermal management of LIBs, there is a growing need for batteries that will be able to work at low, and especially at higher and even extreme temperatures. A lot of research has been done recently covering all battery components mostly up to 55 °C–60 °C, but also at temperatures higher than 100 °C.[21–24]

TiO_2 has already found its application in the field of photocatalysis, solar cells and sensors, and has been investigated as a potential anode material for LIBs for quite some time. Different polymorphs of TiO_2 have been investigated for this purpose and preference is given to the anatase phase, although some studies have emphasized the advantages of the TiO_2(B) phase over anatase.[25–30] TiO_2 is considered as safe anode material with a high Li-ion insertion potential (>1.5 V vs Li/Li^+), non-hazardous handling, low cost, low toxicity, good cycling life and low volume expansion (≈3%) during Li-ion insertion. However, it has low electrical conductivity, and can show poor cycling performance and poor rate capability due to structural changes upon lithiation. Several strategies have been proposed to improve these properties: design of different nanostructures, carbon coating and doping with different atomic species.[17,27,31–38]

An interesting approach towards nanostructured TiO_2 in the form of nanotubes (NTs) or nanotube arrays (NTAs) is their synthesis by simple electrochemical oxidation of Ti foil. Such anodically grown structures provide a unique electrode which combines a TiO_2 intercalation compound, with a Ti current collector without the addition of electronically conductive and adhesive additives. Various applications have been proposed for TiO_2 NTAs and for some of them the dimension of the NTs can be of extreme importance.[14] Lithiation of TiO_2 NTs improves some properties of this material. Meekins and Kamat[39] showed that comparing to untreated Ti/TiO_2 NTAs electrode, lithiation improves photoconversion efficiency (IPCE or external quantum efficiency) 3.5 times at 350 nm. In the investigation our research group conducted with Ti/TiO_2 NTAs electrodes in 2 M NaOH, it was shown that lithiated anatase phase $Li_{0.25}TiO_2$ was a better electrocatalyst for oxygen reduction reaction comparing to both anatase and amorphous TiO_2 NTs.[40] TiO_2 NTs with their tunable diameter and length can offer large exposed surface area and porosity which together with short diffusion length of Li-ion can significantly improve electrochemical performance for an anode in LIBs. The review papers of N.A. Kyeremateng[41] and S. Paul et al.[42] provide an overview of research of TiO_2 NTs for application in 2D and 3D micro-LIBs and LIBs. It is important to stress that, for higher mass loadings of anode, the TiO_2 NTs can be detached from Ti substrate by simple ultrasonication of Ti/TiO_2 NTAs electrode in ethanol.[43] In this way, anodic oxidation of Ti can also be used as a method of synthesis of powdered TiO_2 with nanotube morphology.

In this study we investigated the effect of temperature on the electrochemical performance of anatase TiO_2 NTs by means of cyclic voltammetry (CV), galvanostatic (GS) charge/discharge experiments and electrochemical impedance spectroscopy (EIS) in a temperature range from 25 °C to 55 °C. All electrochemical experiments were performed by using electrodes obtained by anodic

*Electrochemical Society Member.
[z]E-mail: nikola.cvj@ffh.bg.ac.rs

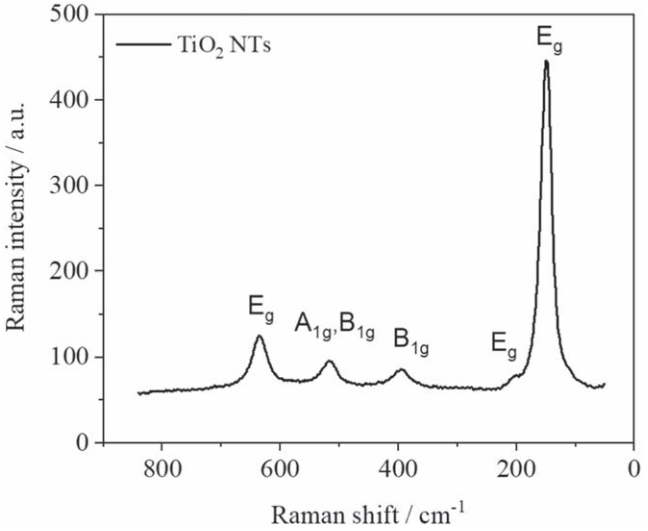

Figure 1. Raman spectra of Ti/TiO_2 NTAs electrode.

oxidation of Ti and additional annealing in order to transform amorphous TiO_2 NTs into the anatase phase. The 1 M solution of $LiClO_4$ in propylene carbonate (PC) was used as an electrolyte. PC was chosen as the solvent because of its high melting and flashing point, which has already been used for high temperature measurements in lithium metal batteries.[23] $LiClO_4$ was chosen as an inexpensive salt whose use in carbonate solutions, most likely, still needs to be re-examined.[44]

Experimental

Material preparation.—TiO_2 NTAs were prepared by anodic oxidation of a 0.25 mm thick and 0.5 cm wide Ti foil (Alfa Aesar, $\omega \geqslant 0.995$). The anodization process took place in an open glass filled with a 0.7% solution of NH_4F in extra pure glycerol (Merck, 99.7%), by using a graphite cathode under constant voltage of 30 V at room temperature for 6 h. Ti-electrodes, covered with TiO_2 NTAs on both sides, were well rinsed with distilled water and dried and subsequently annealed 3 h in air at 400 °C to obtain the TiO_2 anatase phase. In further text, this electrode is designated as Ti/TiO_2 NTAs. The mass of the grown nanotubes on the Ti foil was unknown at the beginning of the experiments, but it was determined at the end of electrochemical experiments by scraping the nanotubes from the foil.

Electrode material characterization.—The presence of anatase phase of anodically grown and additionally annealed TiO_2 NTs was examined by Raman spectroscopy. A Thermo Scientific DXR Raman microscope was employed, using an excitation wavelenght of 532 nm and power of 2 mW. The measurement included 10 s exposure time and a pinhole size of 50 μm.

X-ray diffraction (XRD) patterns of Ti/TiO_2 NTAs electrode and Ti-foil were obtained by Philips PW diffractometer 1050 with Cu-Kα1,2 radiation. XRD data were collected in 2θ range 20°C–80° (2θ), using step size of 0.05° and counting time of 3 s per step.

The morphology and chemical composition of obtained TiO_2 NTAs, as-prepared and after GS cycling experiments, was analyzed by FEI SCIOS 2 dual beam field emission scanning electron microscope (FESEM), equipped with an energy dispersive X-ray spectroscopy (EDS) system.

Infrared (IR) spectra of Ti/TiO_2 NTAs electrode, before and after GS cycling, were recorded with Shimadzu Fourier Transform Infrared (FTIR) Spectrometer with a universal Diamond ATR Sampling Accessory (MIRacle 10 ATR; DIAA/ZnSe) in the range 4000–600 cm^{-1}. After GS cycling the Ti/TiO_2 NTAs electrode was washed with diethyl ether, dried in air and in a stream of argon, before IR spectra recording.

Electrochemical experiments.—CV and EIS experiments were carried out by Potentiostat/Galvanostat/FRA Vertex (Ivium Technologies). A bottle-like three-electrode cell made of Pyrex glass and closed with a Teflon stopper with a double "O" ring was used for CV experiments. Electrical contacts for all three electrodes were routed through the Teflon stopper. The Ti/TiO_2 NTAs electrode was used as a working electrode, while lithium metal foils were used as reference and counter electrodes in the electrochemical cell, filled with about 3 cm^3 of electrolyte, i.e., 1 M solution of $LiClO_4$ in PC. Geometrical surface area of the working electrode in contact with the electrolyte was 1 cm^2. The similar cell, in a two-electrode arrangement, was used for GS charging/discharging experiments performed by Arbin BT 2042 battery testing device. The same two-electrode cell was used for EIS measurements in the frequency range 100000 to 0.01 Hz. All experiments at elevated temperatures were performed using a HAAKE F3 termostat.

Results and Discussion

Electrode material characterisation.—Raman spectra of Ti/TiO_2 NTAs electrode is shown in Fig. 1.

In the Raman spectrum of the TiO_2 NTs five Raman active modes are observed at 148 cm^{-1} (E_g), 204 cm^{-1} (E_g), 394 cm^{-1} (B_{1g}), 515 cm^{-1} (A_{1g}, B_{1g}) and 636 cm^{-1} (E_g), which correspond to the anatase phase.[40,45,46] TiO_2 NTs morphology was investigated by SEM, Figs. 2a–2b.

The NTs are cylindrical in shape with an inner diameter ~95 nm and wall thickness ~15 nm. The nanotubes are not "fused" to each other, having significant space between them. It should be noted that annealing after anodic oxidation and electrochemical experiments do not change the morphology of the NTs, Fig. S1.

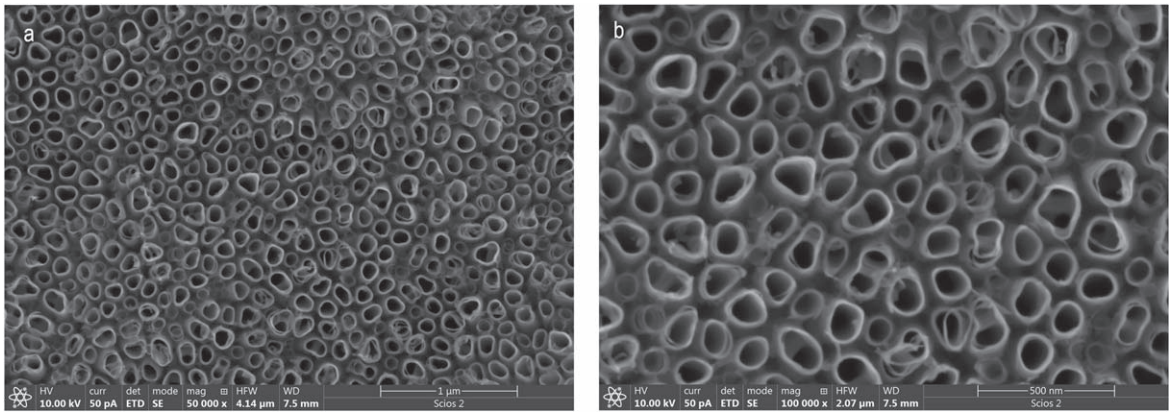

Figure 2. SEM micrographs of Ti/TiO2 NTAs electrode, magnified (a) 50.000 and (b) 100.000 times.

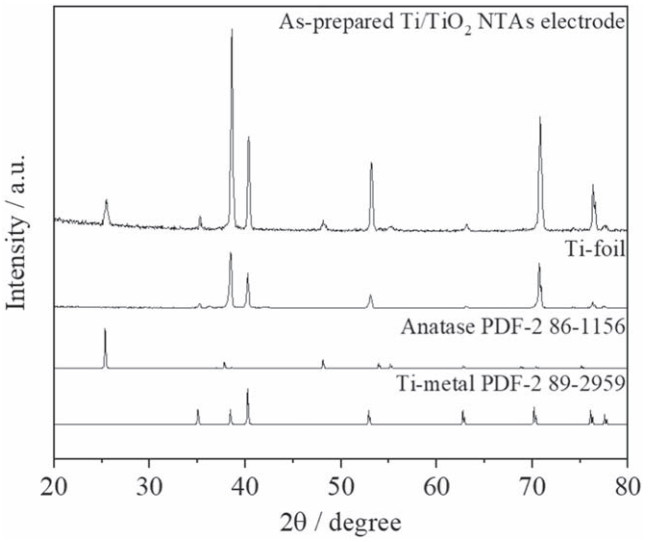

Figure 3. XRD patterns of Ti/TiO_2 NTAs electrode and Ti-foil.

The XRD pattern of Ti/TiO_2 NTAs electrode was recorded to primarily determine the mean crystallite size of anatase phase, synthesized in the form of thin-wall NTs. The obtained pattern contains reflections from both the TiO_2 anatase phase and the Ti-metal phase, as can be seen from Fig. 3, based on comparison with diffractogram of Ti-foil and diffractograms from the XRD database PDF-2.

The strongest diffraction maximum of anatase phase at ~25° (2θ) was used for calculation of the mean crystallite size, applying the XFIT software with a Fundamental Parameters convolution approach to generate line profiles. The obtained value is 19 ± 1 nm. This value of the mean crystallite size is much smaller than the values of 30.6 – 41.3 nm, calculated for TiO_2 anatase NTs with wall thickness of 35–40 nm obtained by anodic oxidation at 20–60 V in our earlier study.[47]

Cyclic voltammetry.—The cyclic voltammograms of Ti/TiO_2 NTAs electrode in 1 M $LiClO_4$/PC solution recorded at scan rates of 5, 10, 20 and 50 $mV \cdot s^{-1}$ are presented in Figs. 4a–4d at temperatures 25 °C–55 °C. In all cases, the upper scan limit of 3.0 V and lower scan limit of 1.0 V were used. Each individual CV curve, in all Figs. 4a–4d, represents the fifth cycle, after which there is no further change in the intensity of the cathodic and anodic peaks.

The presence of characteristic Ti^{4+}/Ti^{3+} strong redox peaks at all scan rates, of which at least the largest ones are not characteristic for organic electrolytes, indicates a fast CV response of Ti/TiO_2 NTAs electrode. The increase in temperature enhances the height of redox peaks, which shows a significant improvement in Li-ion storage capability, Fig. 4. At the same time the peak-to-peak separation ΔE_p decreases, Table S1, indicating better reversibility of Li-ion insertion/deinsertion process, according to theory of reversible and irreversible kinetics of redox reactions in CV.[48] A relatively large ΔE_p which exists here was observed earlier for anatase TiO_2 nanoporous films[36] and nanotubes.[16,47] It could be attributed to the slow electron transfer through semiconducting TiO_2, but according to the research of Vogel et al.[49] this is a more complex issue. An additional cathodic peak of much lower intensity can be observed at more negative potentials, especially at higher temperatures. Although present at all scan rates, this peak is most easily observed at 5 $mV \cdot s^{-1}$, Fig. 4a. Most likely, it can be attributed to additional insertion of Li-ion in orthorhombic Li-titanate phase,[50] whose formation corresponds to the appearance of the strong cathodic peak. In the reverse scan the corresponding oxidation peak appears as a wide peak of very low intensity, easily overlooked, as previously observed in the investigation of TiO_2 NTs of different morphologies.[47]

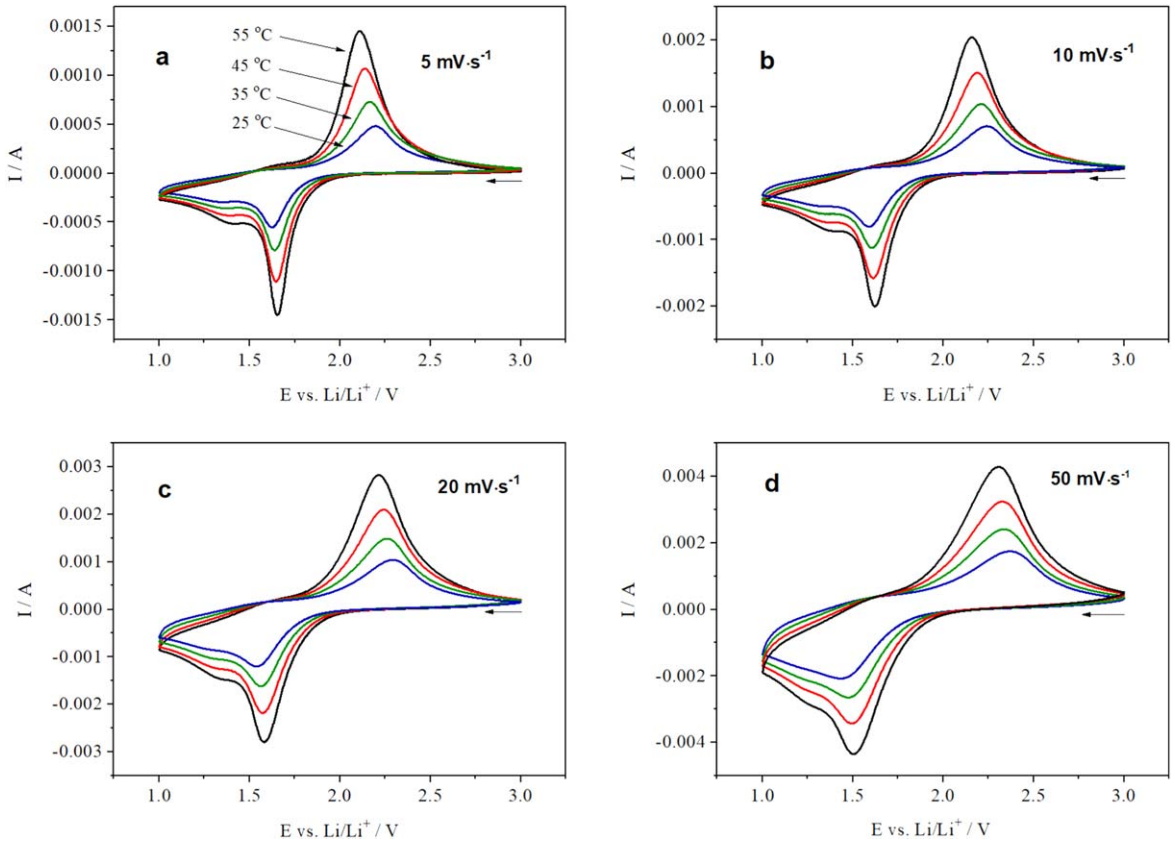

Figure 4. The CV curves of Ti/TiO_2 NTAs electrode recorded at different temperatures at (a) 5 (b) 10 (c) 20 and (d) 50 $mV \cdot s^{-1}$.

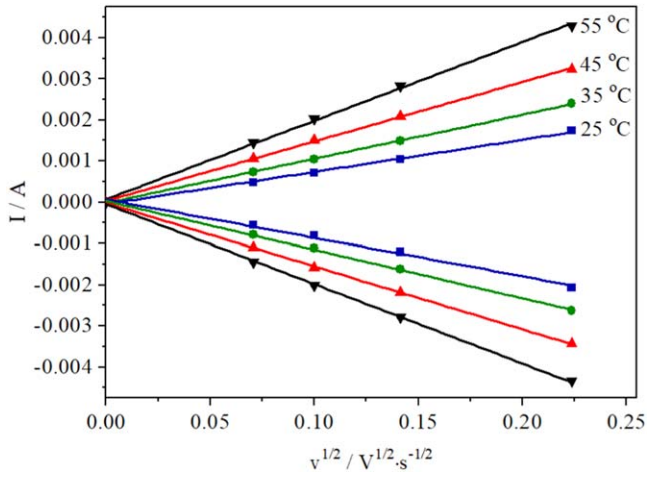

Figure 5. The cathodic and anodic peak current as a function of square root of scan rate at different temperatures.

Table I. Li-ion diffusion coefficients obtained from cyclic voltammetry.

T (°C)	D ($cm^2 \cdot s^{-1}$)	
	Li-ion insertion	Li-ion extraction
25	$8.5 \cdot 10^{-15}$	$6.0 \cdot 10^{-15}$
35	$1.4 \cdot 10^{-14}$	$1.2 \cdot 10^{-14}$
45	$2.5 \cdot 10^{-14}$	$2.2 \cdot 10^{-14}$
55	$4.0 \cdot 10^{-14}$	$3.9 \cdot 10^{-14}$

If peak current is presented as a function of square root of scan rate, at all temperatures the data can be fitted with a straight line with intercept close to zero, Fig. 5.

This indicates the small capacitive contribution to the current at peak maximum. Therefore, the obtained slopes of straight lines were used for calculation of the diffusion coefficients of Li-ion in TiO_2 NTs, at all temperatures, by using the equation for irreversible electrochemical reactions (Eq. S1),[48] which has already been used for such purposes.[36,47,51,52] The obtained diffusion coefficients are shown in Table I.

Values of D from Table I are 5.5–10 times higher comparing to values obtained for TiO_2 NTs, with wall thickness of 35–40 nm and inner diameter 80 nm, which were electrochemically tested using CV at same temperatures in LiTFSI/PYR_{14}TFSI/GBL electrolyte[51] and in a comparative study of LiTFSI/C_2mimTFSI/GBL and LiTFSI/C_2mmimTFSI/GBL electrolytes.[52] The higher diffusion coefficients of Li-ions can be attributed to the shorter diffusion length of thin-wall (~15 nm) TiO_2 NTs obtained and tested in this research.[36,53] Good wetting by the electrolyte from both the inner and outer side of the nanotubes, which is made possible by the resulting morphology, can additionally reduce the diffusion length.

The previous CV investigation of Ti/TiO_2 NTAs electrodes in aforementioned ionic liquid-based electrolytes,[51,52] at the same temperatures and scan rates, showed that capacitive contribution to the current at peaks maxima can be larger than that obtained here. Regardless of this difference, the capacitive contribution to the current in the cyclic voltammograms of TiO_2 anatase, even when it is significant, is the smallest at the maximum of the redox peaks as shown by Laskova et al.[54]

Galvanostatic experiments.—The GS experiments were performed at constant temperature 25 °C with different current rates, Fig. 6a, and with constant current rate at different temperatures i.e. at 25, 35, 45 and 55 °C, Fig. 6b. Current rates were calculated at the end of all GS experiments from the used current densitites (100, 50, 25 and 200 $\mu A \cdot cm^{-2}$) and obtained mass loading of Ti/TiO_2 NTAs electrode, by taking 1 C = 167.5 $mAh \cdot g^{-1}$, which corresponds to the composition of $Li_{0.5}TiO_2$.

GS cycling was first performed at different current rates at 25 °C, Fig. 6a. After an initial capacity drop due to irreversible loss, the lithium insertion/extraction specific capacity becomes very stable at current rate of 5.3 C. At the end of the 50th cycle, the lithiation/delithiation capacity reaches 164.3/162.7 $mAh \cdot g^{-1}$ which corresponds to the Coulumbic efficiency (CE) of 99.0%. By decreasing the current rate to 2.65 C, insertion/extraction capacity increases, remains stable, and reaches a value of 234.4/231.6 $mAh \cdot g^{-1}$ after 25 cycles. CE slightly decreases to 98.8%. Further reduction in current rate to 1.325 C increases discharge/charge capacity which, after a drop of 2–3% during 25 cycles, attains 302.7/297.8 $mAh \cdot g^{-1}$ with corresponding CE of 98.4%. This is a significant improvement in CE compared to 60 V - TiO_2 NTs which show a slightly lower capacity at current rate 1.17 C.[47] With an eight-fold increase of current rate to 10.6 C insertion/deinsertion capacity drops to 113.8/113.6 $mAh \cdot g^{-1}$. The return to 5.3 C gives great stability of lithium insertion/extraction capacity, which is 160.4/160.0 $mAh \cdot g^{-1}$ after 75 cycles at this current rate and a total of 200 cycles at various current rates. Capacity retention in the last 50 cycles is 98.9%. CE is very high at 10.6 C and also after returning to 5.3 C and amounts to 99.8%.

At higher temperatures of 35, 45 and 55 °C the capacity of Ti/TiO2 NTAs electrode was tested during 50 GS cycles at each temperature at current rate of 5.3 C. The final 100 cycles were performed at 25 °C, Fig. 6b. At 35 °C the capacity is very stable during cycling. After 50 cycles lithium insertion/deinsertion capacity is 231.6/230.2 $mAh \cdot g^{-1}$, which gives CE of 99.4%. Lithiation or discharge capacity retention at 35 °C is 98.2%. By increasing the temperature to 45 °C, and subsequently to 55 °C, the capacity continiues to rise. After 50 cycles, at 45 °C and 55 °C, the lithiation/delithiation capacity amounts 299.3/295.4 and 357.3/348.2 $mAh \cdot g^{-1}$, respectively. CE increases from 98.3 to 98.7% at 45 °C and from 96.7 to 97.5% at 55 °C, during GS cycling. At elevated temperatures capacity retention is 98.1–98.5%, Table II. After returning from 55 °C, after 100 cycles at 25 °C, the capacity is 149.3/148.9 $mAh \cdot g^{-1}$, which corresponds to a high CE of 99.7%.

The capacity retention obtained for different cathode materials tested at 55–60 °C (vs graphite, $Li_4Ti_5O_{12}$ or Li anodes) after 50 and 100 cycles was found to be 40%–99% and 75%–97%, respectively.[21,22] The highest values of capacity retention after 50 cycles were obtained for NCM cathode (vs graphite) in the presence of different additives.[22] In this research the specific capacity of thin wall TiO_2 NTs at 55 °C is much higher comparing to cathode materials at similar temperatures presented in these two review articles.[21,22] At 25 °C the lithiation capacity of thin-wall TiO_2 NTs, which is 160.4 $mAh \cdot g^{-1}$ and 113.8 $mAh \cdot g^{-1}$ at current rate 5.3 C and 10.6 C respectively, is similar to capacities of nitrogen doped anatase TiO_2 materials which have high electric conductivity and Li-ion diffusivity. It was found that N-doped hollow urchin like TiO_2@C composite shows lithiation capacity of 164.2 $mAh \cdot g^{-1}$ at 5 C and 111.7 $mAh \cdot g^{-1}$ at 10 C,[55] and the interstitially N-doped INR-TiO_2 delivers 168 $mAh \cdot g^{-1}$ at 5 C and just below 150 $mAh \cdot g^{-1}$ at 10 C.[56] The specific capacity of here tested Ti/TiO_2 NTAs electrode is higher than these powder materials at lower current rates.

Final values of CE show decrease both with increasing temperature and decreasing current rate at 25 °C, Fig. 6. Such decrease can be ascribed most likely to electrolyte decomposition which becomes more intense at elevated temperatures, as well as lower current rates, where Ti/TiO_2 NTAs electrode is a longer time in potential range where decomposition of electrolyte takes place. An increase in the cathodic current approaching the potential of 1.0 V vs Li/Li^+ in cyclic voltammograms, Fig. 4, indicates that possible decomposition of the electrolyte happens near lower cut-off voltage in GS experiments. This kind of behavior has already been observed in our experiments with the same type of electrode in ionic liquid-GBL electrolytes.[51,52] The $LiClO_4$/PC electrolyte, used in this research,

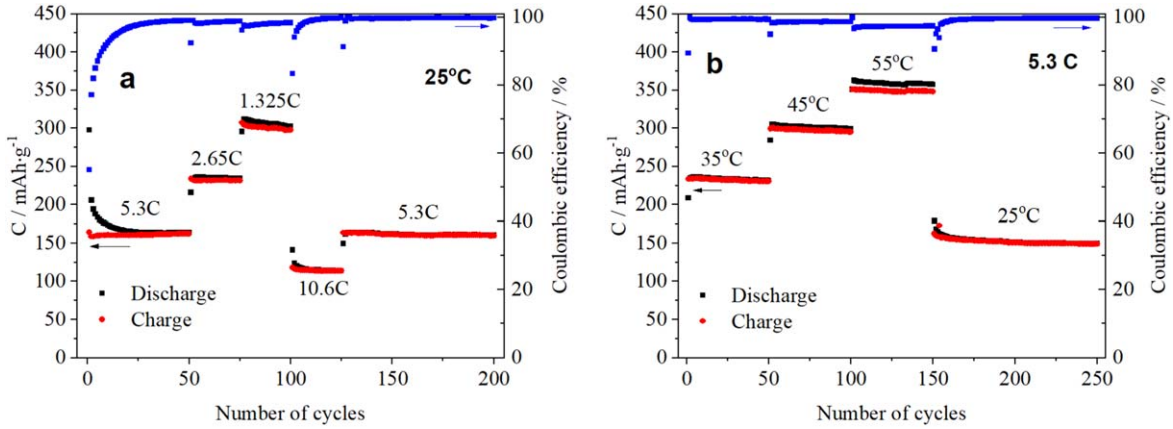

Figure 6. Discharge/charge performance of Ti/TiO_2 NTAs electrode at (a) different current rates at 25 °C and (b) different temperatures at current rate of 5.3 C.

Table II. Galvanostatic performance of Ti/TiO_2 NTAs electrode (vs Li) at different temperatures. At 25 °C cycles 151–200, Fig. 6a, are considered.

T (°C)	Number of cycles	Lithiation capacity (mAh·g^{-1})	Capacity retention (%)	Coulombic efficiency (%)
25	50	160	98.9	99.8
35	50	232	98.2	99.4
45	50	299	98.1	98.7
55	50	357	98.5	97.5

shows lower degree of decomposition comparing to these ionic liquid-GBL electrolytes. It manifests itself through a higher CE comparing to LiTFSI/PYR_{14}TFSI/GBL electrolyte at room temperature[51] and through a higher CE and, above all, a smaller capacity fade at 55 °C comparing to LiTFSI/C_2mimTFSI/GBL and LiTFSI/C_2mmimTFSI/GBL electrolytes.

The voltage profiles at different current rates at 25 °C and at elevated temperatures, Figs. 7a–7c, show several regions.

In discharge, the steep part of the voltage profile which corresponds to small capacities, from ∼3.0 V down to the beginning of flat part region, can be attributed to formation of solid solution domain[57] or capacitive-like surface effect.[58] The flat part of the voltage profile, i.e. voltage plateau (middle part at ∼1.68–1.75 V) reflects transition from lithium-poor $Li_{x1}TiO_2$ phase to lithium-rich $Li_{x2}TiO_2$ phase. x1 is usually taken to be 0.025 or 0.026 and x2 = 0.5–0.55 for micro-sized TiO_2.[37,47,59] The region with inclined voltage profile, down to 1.0 V, designates the existence of surface storage mechanism which leads to pseudo-capacitive behavior.[51,59] Additionally, another region is developing on the inclined part of the discharge profile at ∼1.4–1.5 V. It appears only as inflection point at the highest current rates at 25 °C, but at lower current rates and higher temperatures it actually corresponds to the second voltage plateau that begins to develop. The second voltage plateau represents a phase transition between lithium-rich $Li_{x2}TiO_2$ phase and Li_1TiO_2 phase and generally is characteristic for very small particles and higher temperatures.[59] The surface storage depends on surface area of TiO_2 NTs, but not on solid state diffusion time of Li-ion. The contribution of surface storage to the total capacity is the largest at the highest current rate at 25 °C, and is ∼60%. It decreases with a decrease in current rate, Fig. 7a, and also with an increase in temperature at the constant current rate, Fig. 7b. In the first case the contribution of Li-ion diffusion, i.e. bulk capacity, to the total capacity increases due to the increase in diffusion time, and in the second case because of the increase of diffusion rate. The contribution of the second voltage plateau to overall capacity also increases for the same reasons. However, the contribution of surface storage remains significant and together with the contribution of the second voltage plateau is not less than 40%. The difference in lithiation i.e. discharge capacities of Ti/TiO_2 NTAs electrode at 25 °C before and after GS cycling at 35 °C–55 °C indicates a smaller contribution of surface storage to overall capacity after testing at elevated temperatures, Fig. 7c.

At temperature 45 °C and 55 °C, at relatively high current rate 5.3 C, the end of flat part of voltage plateau in discharge exceeds the value of 184.2 mAh·g^{-1}, which corresponds to the maximum lithium content that is usually taken for micro-sized particles of Li-rich phase $Li_{0.55}TiO_2$, Fig. 7b.[59] According to Figs. 7a and 7b it is reasonable to assume that 184.2 mAh·g^{-1} can be exceeded at much lower current rates at all temperatures used in this investigation. This is possible most likely due to the change of solubility limit. Studies conducted by Mulder's and Wagemaker's research group using ^{7}Li NMR,[60] neutron diffraction,[59] and in situ X-ray diffraction,[37] mostly at room temperature, showed that during lithiation of nanoparticles the phase fraction of Li-rich $Li_{x2}TiO_2$ phase increases mainly by continuous nucleation of new particles rather than concurrent domain growth within the particles. For 7 nm anatase particles Li content can increase up to x2 = 0.74, comparing to 0.55 in microsized $Li_{x2}TiO_2$ phase. Li content in Li-poor $Li_{x1}TiO_2$ phase, for the same particle size, also increases significantly above value of 0.026 and can achieve values up to x1 = 0.21.[59] According to Fig. 7b, further rise in capacity is in connection to the increase in solubility limit at elevated temperatures. What exactly happens during the lithiation of TiO_2 NTs at elevated temperatures remains to be determined by in situ structural investigations.

In here obtained thin-wall NTs the mean crystalline size is 19 nm. For all voltage profiles, Figs. 7a and 7b, at the begining of voltage plateau in charge the potential is not overdriven to higher values than that of the plateau itself.[47] In the case of nanoparticles this would mean the absence of nucleation barrier for the phase transition from Li-rich to Li-poor phase, which further means the absence of Li-rich and Li-poor phase coexistence in single particles. Here, for thin wall nanotubes, with mean crystalline size of 19 nm, this most likely indicates the existence of crystalline domains with either Li-rich or Li-poor phase in which lithium content can be signicifantly increased. In order to see the effect of crystallite size on lithiation capacity, a comparison can be made between thin-wall NTs and NTs with wall thicknesses of 35–40 nm and crystallite sizes 32.3 and 30.6 nm. They were obtained by anodic oxidation at 45 V (45V-NTs) and 60 V

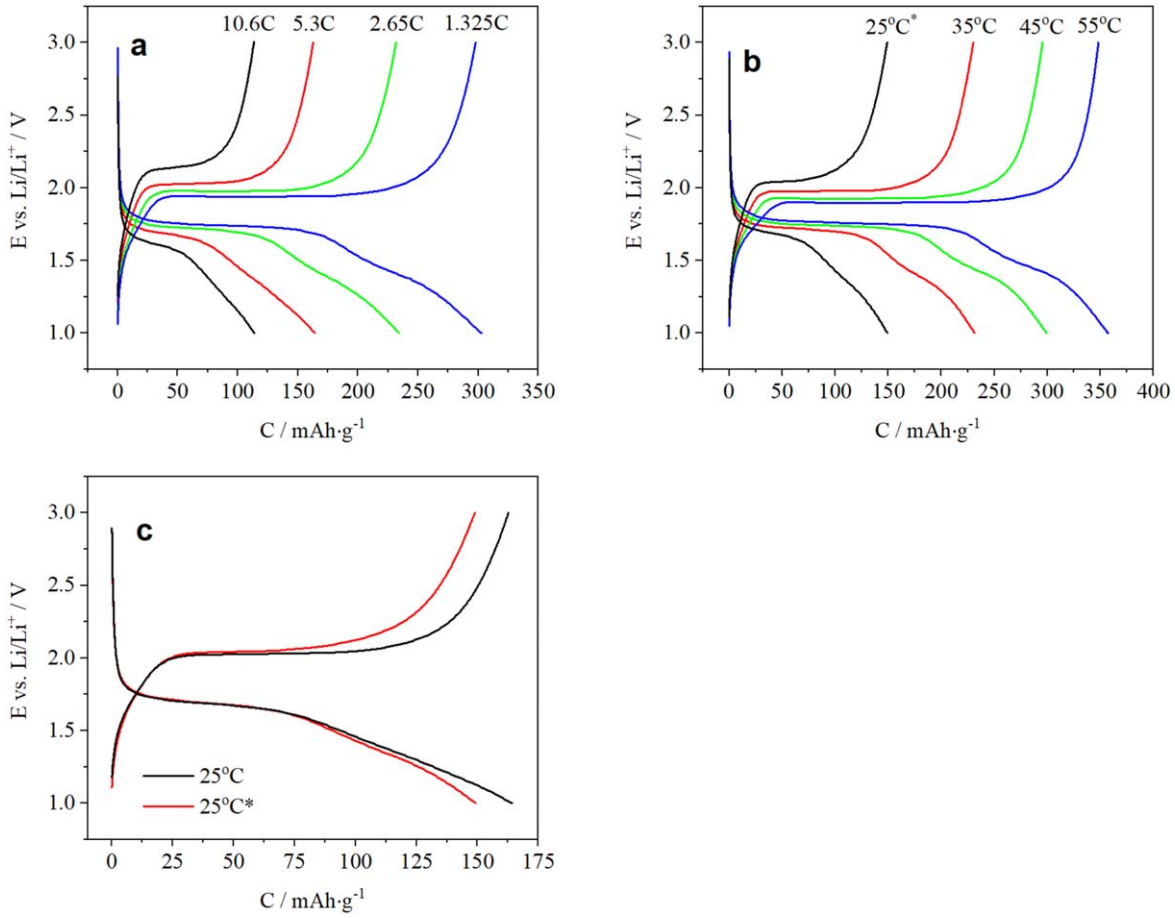

Figure 7. Discharge/charge voltage profiles of Ti/TiO_2 NTAs electrode at (a) different current rates at 25 °C (b) different temperatures at current rate of 5.3 C and (c) Voltage profiles at 25 °C before and after (*) GS cycling at elevated temperatures.

(60V-NTs), respectively, and tested in our earlier investigation.[47] The lithiation capacity of thin-wall NTs electrode at 25 °C, which amounts 303 mAh·g^{-1} at current rate 1.325 C, is significantly higher than 190 mAh·g^{-1} (0.93 C) obtained for 45V-NTs with mean crystallite size of 32.3 nm. For thin-wall NTs and 45V-NTs surface storage capacity contribution to total capacity is similar, however Li-rich and Li-poor phase coexistence in crystalline domains of 45V-NTs gives lower lithium content, while a longer diffusion length is present due to the 35–40 nm thick walls.[37,59] The capacity of 290 mAh·g^{-1} (1.17 C) attained for 60V-NTs comes from very large surface storage capacity contribution to overall capacity due to different morphology comparing to 45V-NTs, regardless of the very small difference in crystallite size.[47] The difference of the total specific capacities of 60V-NTs and thin-wall NTs is very small, but the capacity of thin-wall NTs prevails due to the higher lithium solubility limit in 19 nm crystallites and shorter diffusion length. Anwar et al.[61] investigated the influence of crystallite size on lithiation/delithiation capacity of NTs with a very small difference in morphology obtained by annealing amorphous TiO_2 in different atmospheres. They found that the decrease of mean crystalline size from 33 to 27 nm increases lithium insertion capacity from 165 to 190 mAh·g^{-1} at current rate of 0.1 C.

EIS measurements.—EIS measurements were performed at 25 °C–55 °C by using the same two-electrode cell as for GS cycling. Before EIS measurements, at each temperature the Ti/TiO_2 NTAs electrode was galvanostatically lithiated, then half-delithiated and allowed to relax until constant potential is reached. At 25 °C EIS spectra were recorded after 200 GS cycles, Fig. 6a, and again, after returning from 55 °C, after 75 cycles, Fig. 6b. At elevated temperatures impedance measurements were performed after 50 GS cycles. Nyquist plots obtained at all temperatures are presented in Figs. 8a–8e. The same equivalent circuit, presented in the inset of Figs. 8a–8e, was used for fitting EIS data at all temperatures.

The depressed semicircle in the higher frequency region of the Nyquist plot originates from the formation of SEI layer. This semicircle is modeled with constant phase element (CPE_1) and SEI layer resistance, R_{SEI}, in parallel. Its high-frequency intersection with the *x*-axis gives the electrolyte resistance R_e. In the middle-frequency and low-frequency region data are modeled by using modified Randles circuit, which combines charge transfer impedance (the second depressed semicircle, elements CPE_2 and R_{ct}) with Warburg diffusional impedance (the stright line of unit slope, element W). The overlapping of the second depressed semicircle with linear part is present at all temperatures, but decreases with increasing temperature, Fig. 8. The greater overlapping indicates the existence of larger mixed kinetic and diffusion control of lithium ion insertion. The resistances obtained as a result of data fitting are shown in Table III.

The change of the electrolyte resistance R_e with increasing temperature shows the expected increase of electrolyte conductivity, which is at 55 °C approximately two times higher than the initial value at 25 °C. The SEI layer resistivity R_{SEI} drops approximately twice when temperature rises from 25 to 35 °C and from 35 to 45 °C and then only ∼5% with the increase in temperature to 55 °C. Returning to 25 °C, the value of R_{SEI} is ∼29% lower than the initial value at the same temperature, which most likely indicates a change in the composition of the SEI layer. The charge transfer resistance R_{ct} decreases 10 times with increasing temperature up to 55 °C. An increase in temperature leads to a large drop in all resistances, as

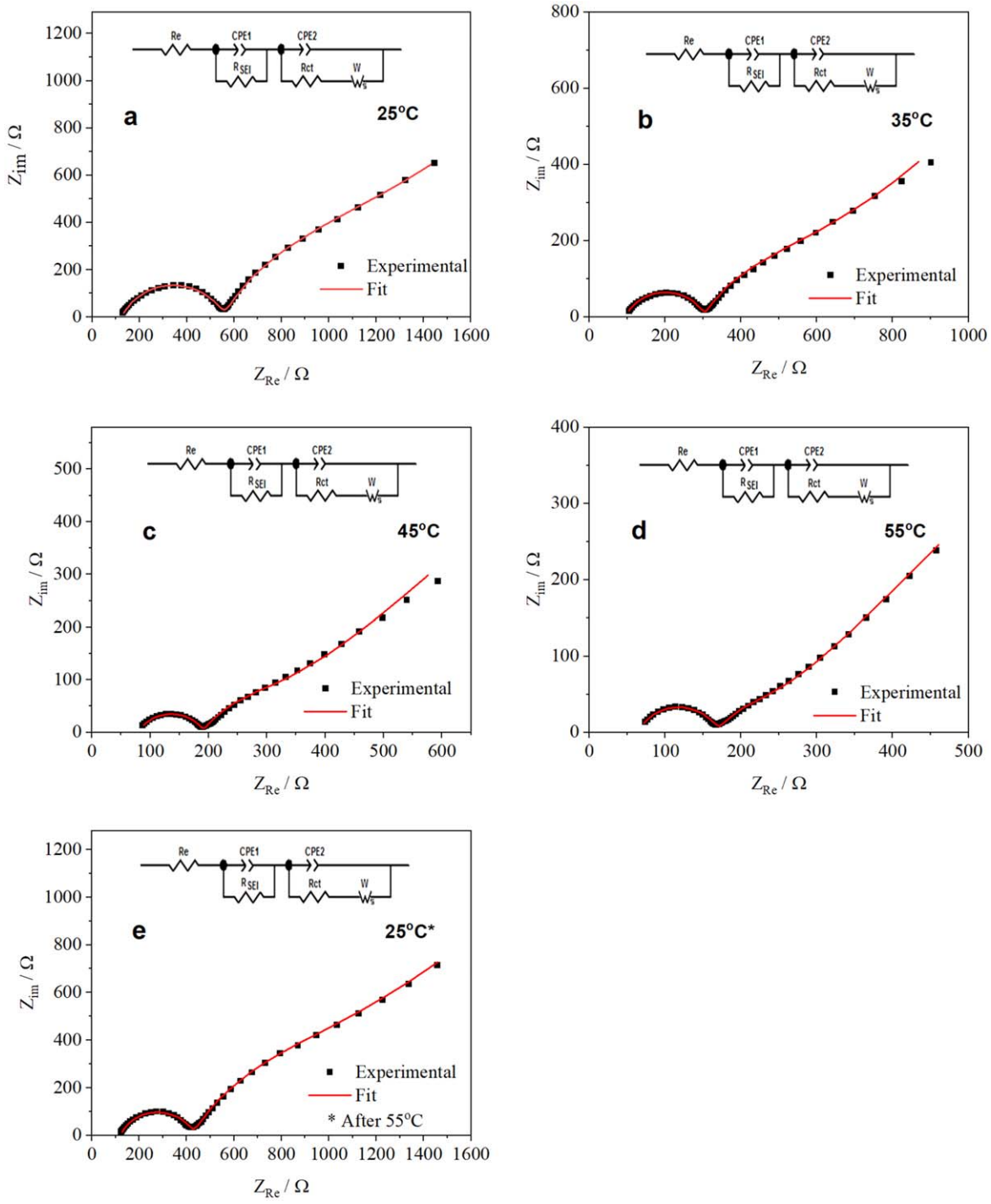

Figure 8. Nyquist plots obtained by EIS for Ti/TiO_2 NTAs electrode at (a) 25 (b) 35 (c) 45 (d) 55 and (e) 25 °C (after 55 °C).

well as to an increase in the diffusion coefficient D of Li-ions in TiO_2 NTs, Table III. This significantly contributes to the increase in total capacity of TiO_2 NTs with temperature rise. It is interesting that values of D obtained from EIS, Table III, are three orders of magnitude lower than those obtained from CV, Table I. The main difference between these two methods is that in the EIS method the investigated electrode is slightly perturbed from its equilibrium potential, while in the CV method it is under dynamic conditions of potential change. According to mini-review about applications of voltammetry in Li-ion battery research, the use of high scan rates in

Table III. Resistances and Li-ion diffusion coefficients obtained from EIS data fitting.

T (°C)	R_e (Ω)	R_{SEI} (Ω)	R_{ct} (Ω)	D ($cm^2 \cdot s^{-1}$)
25	125	435	950	$5.2 \cdot 10^{-18}$
35	95	210	420	$1.3 \cdot 10^{-17}$
45	80	112	185	$3.4 \cdot 10^{-17}$
55	64	107	94	$7.1 \cdot 10^{-17}$
25*	120	310	950	$5.0 \cdot 10^{-18}$

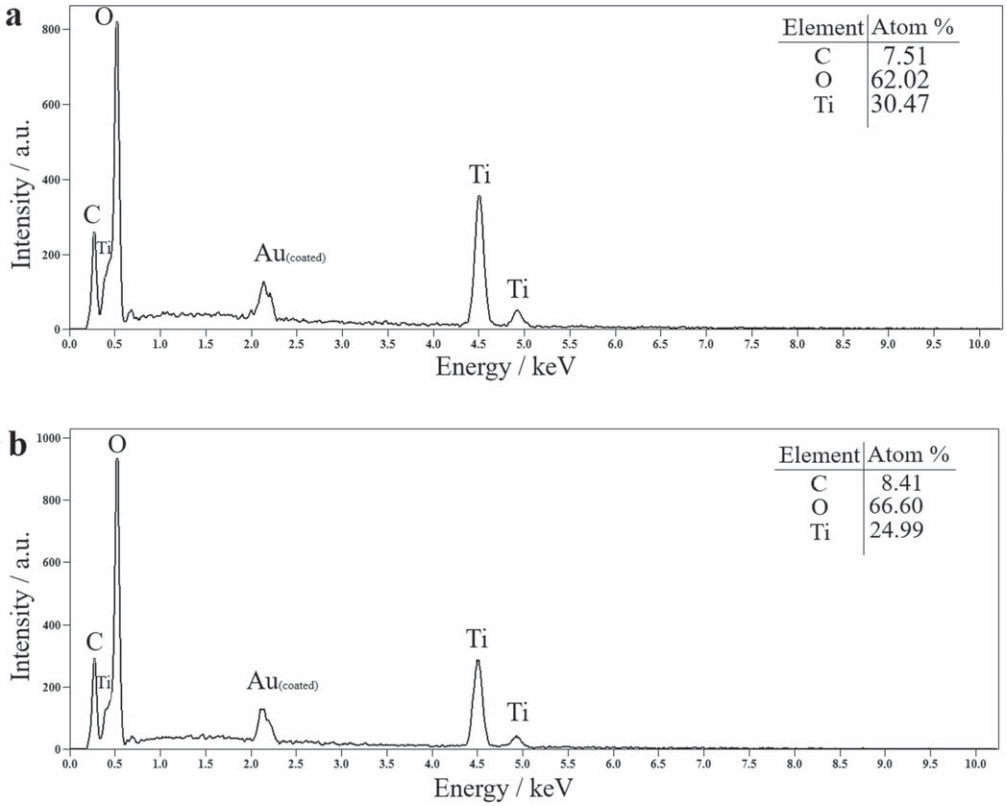

Figure 9. EDS analysis of (a) as-prepared electrode and (b) electrode after GS cycling.

CV, above 2 mV·s^{-1}, tends to generate large potential gradients in the active material, which greatly overestimates D.[53]

EDS and FTIR spectra.—In order to investigate the nature of SEI film, EDS and FTIR spectra of Ti/TiO2 NTAs electrode were recorded before and after GS cycling experiments.

The elemental composition of electrode surface was investigated with EDS, Fig. 9.

For as-prepared electrode the EDS analysis confirmed closely the composition (in atomic %) of TiO_2 NTs, Fig. 9a. Complex peak of relatively small intensity, slightly above 2 keV, comes from Au-coating. Although the newly prepared electrode does not contain carbon, its presence in the SEM-EDS system comes from high background counts. EDS spectrum of Ti/TiO2 NTAs electrode after GS cycling experiments shows the increased content of oxygen and carbon comparing to titanium, Fig. 9b, Table S2. According to the values obtained, 16.6 atomic % of oxygen and 6.41 atomic % of carbon could be attributed to the SEI layer, given that 50 atomic % of oxygen belongs to TiO_2 and that the background C in this case was much lower, only 2 atomic %. This gives a ratio of the number of oxygen to carbon atoms in the SEI layer of ~2.6.

FTIR spectra are presented in Fig. 10 in frequency range 1600–600 cm^{-1}. At higher frequencies, it is difficult to single out the vibration bands with certainty due to the low signal-to-noise ratio, Fig. S5.

IR vibrational bands at 861, 1427 and 1509 cm^{-1} are clearly visible for Ti/TiO2 NTAs electrode after GS cycling and are absent in the spectrum of the electrode not subjected to electrochemical experiments, Fig. 10. Bands at similar wavenumbers, 1420 and 1510 cm^{-1}, had been observed (at 870 cm^{-1} only mentioned) as a result of cathodic decomposition of PC, and attributed to CO_3^{2-} anion in the paper of Kavan et al.[62] The main IR bands of CO_3^{2-} appear at 1450–1410 cm^{-1} and 880–800 cm^{-1}.[63] In here obtained spectrum the IR band at 861 cm^{-1} originates from asymmetric deformation vibration CO_3^{2-}. The bands at 1427 and 1509 cm^{-1} can

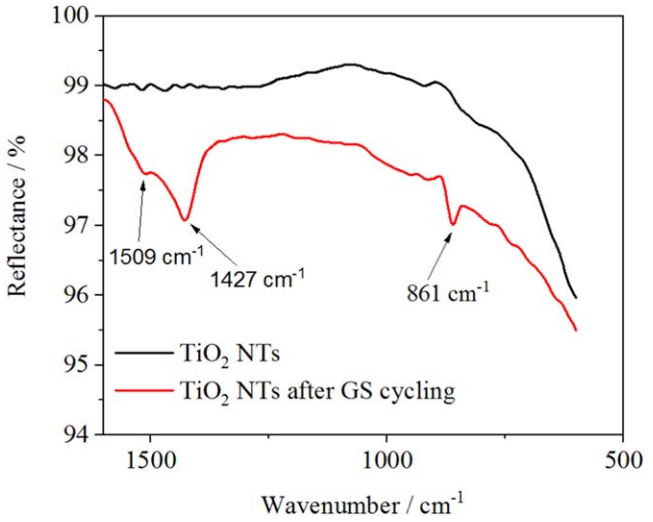

Figure 10. FTIR spectrum (1600 – 600 cm^{-1}) of Ti/TiO_2 NTAs electrode before GS cycling and after.

be ascribed to monodentate carbonates in which bent CO_2 molecule is bonded to a surface oxygen atom through the central carbon atom.[64] Such structures, most likely form SEI layer.

Despite the excellent capacity values of thin-wall TiO2 NTs, it is possible to further improve the performance of Ti/TiO_2 NTAs//$LiClO_4$/PC half-cell. This would primarily refer to the enhancement of CE and capacity retention due to the intensification of electrolyte decomposition at higher temperatures. Recently, investigation by our research group has shown how zwitterionic additive can drastically improve GS cycling properties of Ti/TiO_2 NTAs electrode in ionic liquid-based electrolyte.[65] For obtaining

large capacity values at very high current rates, up to 100 C, interstitial N-doping of TiO_2 NTs would probably be a good option.[56]

Conclusions

Lithiation/delithiation properties of anatase TiO_2 in the form of thin-wall nanotubes were tested at temperatures 25 °C–55 °C by using Ti/TiO_2 NTAs electrode. At 25 °C, a particularly large capacity value of 303 mAh·g^{-1} was obtained at the lowest tested current rate 1.325 C, but at higher current rates the capacity retention and Coulombic efficiency were better. At elevated temperatures very large capacity values were obtained, at relatively high current rate 5.3 C. The lithiation capacity at 55 °C was 357 mAh·g^{-1}, which is more than twice as high as at 25 °C. A Ti/TiO2 NTAs electrode with such a large capacity could be used for 2D micro-batteries for applications at elevated temperatures. The high capacity values of thin-wall TiO_2 NTs can be attributed to the short diffusion length of Li-ion, a small crystallite size, the large contribution of surface storage and the development of a second voltage plateau. Surface storage contributed more at higher current rates and lower temperatures, and the second voltage plateau was more pronounced at lower current rates and higher temperatures. A very large drop of SEI layer resistance and charge transfer resistance, together with the increase of Li-ion diffusion coefficient, also strongly contributed to high total capacity values at elevated temperatures. While capacity retention was 98.1%–98.9%, Coulombic efficiency decreased with increasing temperature and reached the lowest value of 97.5% at 55 °C, when electrolyte decomposition was most pronounced. Most likely, both capacity retention and Coulombic efficiency of TiO_2 anode can be significantly improved by using a well-designed additive in the propylene carbonate-based electrolyte.

Acknowledgments

Funding: The Ministry of Science, Technological Development and Inovation (Republic of Serbia) financially supported this project (contract number: 451–03–47/2023–01/200146). We want to express our gratitude to Dr. Dragana Jugović, from Institute of Technical Sciences of the Serbian Academy of Sciences and Arts, University of Belgrade, Serbia, for her help with the XRD experiments, Dr. Danica Bajuk-Bogdanović, from University of Belgrade—Faculty of Physical Chemistry, Belgrade, Serbia, for recording Raman and FTIR spectra and to Dr. Vladimir Rajić, from Department of Atomic Physics, Vinča Institute of Nuclear Sciences - National Institute of the Republic of Serbia, University of Belgrade, Serbia, for recording SEM micrographs.

ORCID

Nemanja Latas https://orcid.org/0000-0002-5708-5055
Nikola Cvjetićanin https://orcid.org/0000-0001-9350-4010

References

1. J. B. Goodenough and K. S. Park, "The Li-ion rechargeable battery: a perspective." *J. Am. Chem. Soc.*, **135**, 1167 (2013).
2. B. Scrosati and J. Garche, "Lithium batteries: Status, prospects and future." *J. Power Sources*, **195**, 2419 (2010).
3. G. Zubi, R. Dufo-López, M. Carvalho, and G. Pasaoglu, "The lithium-ion battery: State of the art and future perspectives." *Renewable Sustainable Energy Rev.*, **89**, 292 (2018).
4. H. Chen, A. Abidi, A. K. Hussein, O. Younis, M. Degani, and B. Heidarshenas, "Investigation of the use of extended surfaces in paraffin wax phase change material in thermal management of a cylindrical lithium-ion battery: Applicable in the aerospace industry." *J. Energy Storage*, **45**, 103685 (2022).
5. M. Armand and J. M. Tarascon, "Building better batteries." *Nature*, **451**, 652 (2008).
6. J. Piatek, S. Afyon, T. M. Budnyak, S. Budnyk, M. H. Sipponen, and A. Slabon, "Sustainable li-ion batteries: chemistry and recycling." *Adv. Energy Mater.*, **11**, 2003456 (2020).
7. M. S. Whittingham, "Special editorial perspective: Beyond Li-ion battery chemistry." *Chem. Rev.*, **120**, 6328 (2020).
8. H. Liu, X. Shi, Y. Zhang, A. Song, J. Chai, L. Zhang, and J. Zhang, "$Li_4Mo_4O_{17}$ micron particles as new high-performance anode materials for lithium-ion batteries." *Mater. Lett.*, **305**, 130803 (2021).
9. X. Zeng, Q. Kuang, Q. Fan, Y. Dong, Y. Zhao, S. Chen, and S. Liu, "Synthesis, structure and electrochemical performance of V_3BO_6 nanocomposite: A new vanadium borate as high-rate anode for Li-ion batteries." *Electrochim. Acta*, **335**, 135661 (2020).
10. M. M. Thackeray and K. Amine, "$Li_4Ti_5O_{12}$ spinel anodes." *Nat. Energy*, **6**, 683 (2021).
11. J. Wang, H. Zhao, Z. Li, Y. Wen, Q. Xia, Y. Zhang, and G. Yushin, "Revealing rate limitations in nanocrystalline $Li_4Ti_5O_{12}$ anodes for high-power lithium ion batteries." *Adv. Mater. Interfaces*, **1**, 1600003 (2016).
12. M. Liu, C. Yan, and Y. Zhang, "Fabrication of Nb_2O_5 nanosheets for high-rate lithium ion storage applications." *Sci. Rep.*, **5**, 8326 (2015).
13. V. Aravindan, W. C. Ling, and S. Madhavi, "$LiCrTiO_4$: A high-performance insertion anode for lithium-ion batteries." *ChemPhysChem*, **13**, 3263 (2012).
14. P. Roy, S. Berger, and P. Schmuki, "TiO_2 nanotubes: synthesis and applications." *Angew. Chem. Int. Ed. Engl.*, **50**, 2904 (2011).
15. Y. Xu, E. M. Lotfabad, H. Wang, B. Farbod, Z. Xu, A. Kohandehghan, and D. Mitlin, "Nanocrystalline anatase TiO_2: a new anode material for rechargeable sodium ion batteries." *ChemComm*, **49**, 8973 (2013).
16. S. G. Park, J. J. Yang, J. W. Rho, H. I. Kim, and H. Habazaki, "Electrochemical behavior of TiO_2 nanotube/Ti prepared by anodizing for micro-lithium ion batteries." *J. Korean Electrochem. Soc.*, **17**, 13 (2014).
17. H. M. Ali, *Titanium Dioxide—Advances and Aplications* (IntechOpen, London) Chap. 8 (2022).
18. R. Tao et al., "Insight into the fast-rechargeability of a novel $Mo_{1.5}W_{1.5}Nb_{14}O_{44}$ anode material for high-performance lithium-ion batteries." *Adv. Energy Mater.*, **12**, 2200519 (2022).
19. S. Ma, M. Jiang, P. Tao, C. Song, J. Wu, J. Wang, T. Deng, and W. Shang, "Temperature effect and thermal impact I lithium-ion batteries: A review." *Prog. Nat. Sci.*, **28**, 653 (2018).
20. X. Zhang, Z. Li, L. Luo, Y. Fan, and Z. Du, "A review on thermal management of lithium-ion batteries for electric vehicles." *Energy*, **238**, 121652 (2022).
21. M.-T. F. Rodrigues, G. Babu, H. Gullapalli, K. Kalaga, F. N. Sayed, K. Kato, J. Joyner, and P. M. Ajayan, "A materials perspective on Li-ion batteries at extreme temperatures." *Nat. Energy*, **2**, 17108 (2017).
22. D. R. Wright, N. Garcia-Areaz, and J. R. Owen, "Review on high temperature secondary Li-ion batteries." *Energy Procedia*, **151**, 174 (2018).
23. Z. Geng, J. Lu, Q. Li, J. Qiu, Y. Wang, J. Peng, J. Huang, W. Li, X. Yu, and H. Li, "Lithium metal batteries capable of stable operation at elevated temperature." *Energy Storage Mater.*, **23**, 646 (2019).
24. G. Cai, J. Holoubek, M. Li, H. Gao, Y. Yin, S. Yu, H. Liu, T. A. Pascal, P. Liu, and Z. Chen, "Solvent selection criteria for temperature-resilient lithium–sulfur batteries." *Proc. Natl Acad. Sci. USA*, **119**, 2200392119 (2022).
25. B. Z. Christansen, K. West, T. Jacobsen, and S. Atlung, "Lithium insertion in different TiO_2 modifications." *Solid State Ion.*, **28**, 1176 (1988).
26. G. Armstrong, A. R. Armstrong, and P. G. Bruce, "TiO_2(B) nanowires as an improved anode material for lithium-ion batteries containing $LiFePO_4$ or $LiNi_{0.5}Mn_{1.5}O_4$ cathodes and a polymer electrolyte." *Adv. Mater.*, **18**, 2597 (2006).
27. L. Kavan, "Lithium insertion into TiO_2 (anatase): electrochemistry, Raman spectroscopy, and isotope labeling." *J. Solid State Electrochem.*, **18**, 2297 (2014).
28. M. Pfanzelt, P. Kubiak, M. Fleischhammer, and M. Wohlfahrt-Mehrens, "TiO_2 rutile — An alternative anode material for safe lithium-ion batteries." *J. Power Sources*, **196**, 6815 (2011).
29. A. G. Dylla, G. Henkelman, and K. J. Stevenson, "Lithium insertion in nanostructured TiO_2(B) architectures." *Acc. Chem. Res.*, **46**, 1104 (2013).
30. V. Aravidan, Y.-S. Lee, R. Yazami, and S. Madhavi, "TiO_2 polymorphs in 'rocking - chair' Li-ion batteries." *Mater. Today*, **18**, 345 (2015).
31. X. Yang, D. Tang, B. Liu, Y. Yu, and X. Yang, "Nanosized anatase titanium dioxide loaded porous carbon nanofiber webs as anode materials for lithium-ion batteries." *Electrochem. Commun.*, **13**, 1098 (2011).
32. H. Qiao, L. Xiao, and L. Zhang, "Phosphorization: a promising approach to enhance the performance of mesoporous TiO_2 anode for lithium ion batteries." *Electrochem. Commun.*, **10**, 616 (2008).
33. D. H. Lee, B. H. Lee, A. K. Sinha, J. H. Park, M. S. Kim, J. Park, H. Shin, K. S. Lee, Y. E. Sung, and T. Hyeon, "Engineering titanium dioxide nanostructures for enhanced lithium-ion storage." *J. Am. Chem. Soc.*, **140**, 16676 (2018).
34. V. Subramanian, A. Karki, K. I. Gnanasekar, F. P. Eddy, and B. Rambabu, "Nanocrystalline TiO_2 (anatase) for Li-ion batteries." *J. Power Sources*, **159**, 186 (2006).
35. H. T. Fang, M. Liu, D. W. Wang, T. Sun, D. S. Guan, F. Li, J. Zhou, T. K. Sham, and H. M. Cheng, "Comparison of the rate capability of nanostructured amorphous and anatase TiO_2 for lithium insertion using anodic TiO_2 nanotube arrays." *Nanotechnology*, **20**, 225701 (2009).
36. H. Lindstrom, S. Sodergren, A. Solbrand, H. Rensmo, J. Hjelm, A. Hagfeldt, and S. E. Lindquist, "Li^+ ion insertion in TiO_2 (Anatase). 2. voltammetry of nanoporous films." *J. Phys. Chem. B*, **101**, 7717 (1997).
37. K. Shen, H. Chen, F. Klaver, F. M. Mulder, and M. Wagemaker, "Impact of particle size on the non-equilibrium phase transition of lithium-inserted anatase TiO_2." *Chem. Mater.*, **26**, 1608 (2014).
38. J. S. Chen and X. W. Lou, "Anatase TiO_2 nanosheet: An ideal host structure for fast and efficient lithium insertion/extraction." *Electrochem. Commun.*, **11**, 2332 (2009).
39. B. H. Meekins and P. V. Kamat, "Got TiO_2 nanotubes? Lithium ion intercalation can boost their photoelectrochemical performance." *ASC Nano*, **3**, 3437 (2009).

40. J. Milkić, S. Marić, N. Cvjetićanin, Z. Dohčević-Mitrović, and B. Šljukić, "Facile preparation and high activity of TiO_2 nanotube arrays toward oxygen reduction in alkaline media." *J. Electrochem. Soc.*, **165**, 3253 (2018).
41. N. A. Kyeremateng, "Self-organised TiO2 nanotubes for 2D or 3D Li-Ion Microbatteries." *ChemElectroChem*, **1**, 1442 (2014).
42. S. Paul, M. A. Rahman, S. B. Sharif, J.-H. Kim, S.-E.-T. Siddiqui, and M. A. M. Hossain, "TiO_2 as an anode of high-performance lithium-ion batteries: a comprehensive review towards practical application." *Nanomaterials*, **12**, 2034 (2022).
43. J. Lin, X. Liu, S. Zhu, Y. Liu, and X. Chen, "Anatase TiO2 nanotube powder film with high crystallinity for enhanced photocatalytic performance." *Nanoscale Res. Lett.*, **10**, 110 (2015).
44. R. Marom, O. Haik, D. Aurbach, and I. C. Halalay, "Revisiting $LiClO_4$ as an electrolyte for rechargeable lithium-ion batteries." *J. Electrochem. Soc.*, **157**, A972 (2010).
45. J. Zhang, M. Li, Z. Feng, J. Chen, C. Li, and U. V. Raman, "spectroscopic study on TiO2. I. Phase transformation at the surface and in the bulk." *J. Phys. Chem. B*, **110**, 927 (2006).
46. T. Ohsaka, F. Izumi, and Y. Fujiki, "Raman spectrum of anatase, TiO2." *J. Raman Spectrosc.*, **7**, 321 (1978).
47. M. Bratić, D. Jugović, M. Mitrić, and N. Cvjetićanin, "Insertion of lithium ion in anatase TiO_2 nanotube array of different morphology." *J. Alloys Compd.*, **712**, 90 (2017).
48. A. J. Bard and L. R. Faulkner, *Electrochemical Methods: Fundamentals and Applications* (Wiley, New York) 2nd ed., p. 226 (2001).
49. Y. B. Vogel, A. Molina, J. Gonzalez, and S. Ciamp, "Quantitative analysis of cyclic voltammetry of redox monolayers adsorbed on semiconductors: isolating electrode kinetics, lateral interactions, and diode currents." *Anal. Chem.*, **91**, 5929 (2019).
50. M. Wagemaker, G. J. Kearley, A. A. van Well, H. Mutka, and F. M. Mulder, "Multiple Li positions inside oxygen octahedra in lithiated TiO_2 anatase." *J. Am. Chem. Soc.*, **125**, 840 (2003).
51. N. Zec, N. Cvjetićanin, M. Bešter-Rogač, M. Vraneš, and S. Gadžurić, "Electrochemical performance of anatase TiO_2 nanotube arrays electrode in ionic liquid based electrolyte for lithium ion batteries." *J. Electrochem. Soc.*, **164**, H5100 (2017).
52. S. Papović, N. Cvjetićanin, S. Gadžurić, M. Bešter-Rogač, and M. Vraneš, "N., Physicochemical and electrochemical characterization of imidazolium based IL + GBL mixtures as electrolytes for lithium-ion batteries." *Phys. Chem. Chem. Phys.*, **19**, 28139 (2017).
53. T. Kim, W. Choi, H.-C. Chin, J.-Y. Choi, J. M. Kim, M.-S. Park, and W.-S. Yoon, "Application of voltammetry in lithium ion battery research." *J. Electrochem. Sci. Technol.*, **11**, 14 (2020).
54. B. Laskova, M. Zukalova, A. Zukala, M. Bousa, and L. Kavan, "Capacitive contribution to Li-storage in TiO2 (B) and TiO2 (anatase)." *J. Power Sources*, **246**, 103 (2014).
55. Y. Xing, S. Wang, B. Fang, G. Song, D. P. Wilkinson, and S. Yhang, "N-doped hollow urchin like TiO_2@C composite as a novel anode for Li-ion batteries." *J. Power Sources*, **385**, 10 (2018).
56. W. H. Choi, C. H. Lee, H. Kim, S. U. Lee, and J. H. Bang, "Designing a high-performance nitrogen-doped titanium dioxide anode material for lithium-ion batteries by unravelling the nitrogen doping effect." *Nano Energy*, **74**, 104829 (2020).
57. G. Sudant, E. Baudrin, D. Larcher, and J.-M. Tarascon, "Electrochemical lithium reactivity with nanotextured anatase-type TiO_2." *J. Mater. Chem.*, **15**, 1263 (2005).
58. C. Jiang, M. Wei, Z. Qi, T. Kudo, I. Honma, and H. Zhou, "Particle size dependence of the lithium storage capability and high rate performance of nanocrystalline anatase TiO_2 electrode." *J. Power Sources*, **166**, 239 (2007).
59. M. Wagemaker, W. J. H. Borghols, and F. M. Mulder, "Large impact of particle size on insertion reactions. A case for anatase Li_xTiO_2." *J. Am. Chem. Soc.*, **129**, 4323 (2007).
60. M. Wagemaker, R. van de Krol, A. P. M. Kentgens, A. A. van Well, and F. M. Mulder, "Two Phase morphology limits lithium diffusion in TiO2 (Anatase): A ^{7}Li MAS NMR Study." *J. Am. Chem. Soc.*, **123**, 11454 (2001).
61. T. Anwar, W. Li, N. Hussain, W. Chen, R. U. R. Sagar, and L. Tongxiang, "Effect of annealing atmosphere induced crystallite size changes on the electrochemical properties of TiO_2 nanotube arrays." *J. Elect. Eng.*, **4**, 43 (2016).
62. L. Kavan, K. Kartochvilova, and M. Gratzel, "Study of nanocrystalline TiO_2 (anatase) electrode in the accumulation regime." *J. Electroanal. Chem.*, **394**, 93 (1995).
63. B. Stuart, *Infrared Spectroscopy: Fundamentals and Applications* (Wiley, New York), p. 95 (2004).
64. U. Tumuluri, J. D. Howe, W. P. Mounfield III, M. Li, M. Chi, Z. D. Hood, K. S. Walton, D. S. Sholl, S. Dai, and Z. Wu, "Effect of surface structure of TiO_2 nanoparticles on CO_2 adsorption and SO_2 resistance." *ACS Sustain. Chem. Eng.*, **5**, 9295 (2017).
65. A. Roganović, M. Vraneš, N. Cvjetićanin, X. Chen, and Snežana Papović, "Effect of zwitterionic additive on electrode protection through electrochemical performances of anatase tio_2 nanotube array electrode in ionic liquid electrolyte." *Int. J. Mol. Sci.*, **24**, 3495 (2023).